J. Appl. Comput. Mech., 5(2) (2019) 441-453
DOI: 10.22055/JACM.2018.27138.1380

ISSN: 2383-4536
jacm.scu.ac.ir

M&MoCS

Shahid Chamran University of Ahvaz

Journal of Applied and Computational Mechanics

Research Paper

Variable Thermal Conductivity and Thermal Radiation Effect on the Motion of a Micro Polar Fluid over an Upper Surface

G. Sarojamma[1], R. Vijaya Lakshmi[1], P. V. Satya Narayana[2], K. Vajravelu[3]

[1] Department of Applied Mathematics, Sri Padmavati Mahila University
Tirupati,Andhra Pradesh -517502, India, Emails: sarojamma@spmvv.ac.in
[2] Department of Mathematics, SAS, VIT
Vellore,Tamil Nadu-632014, India, Email: psatya@vit.ac.in
[3] Department of Mathematics, University of Central Florida
Orlando, FL 32816, USA, Email: kuppalapalle.vajravelu@ucf.edu

Received September 21 2018; Revised December 22 2018; Accepted for publication December 22 2018.
Corresponding author: G. Sarojamma, sarojamma@spmvv.ac.in

Abstract: The intent of this analysis is to explore the influence of thermal radiation paired with variable thermal conductivity on MHD micropolar fluid flow over an upper surface. The novelty of the present model is to consider the fluid flow along an upper horizontal surface of a paraboloid of revolution (*uhspr*) with the porous medium. This physical phenomenon is described by a set of coupled non-linear ODEs by using suitable scaling analysis. The ODEs along with the boundary conditions are solved numerically. Influence of various flow parameters on momentum, thermal and concentration boundary layers is discussed graphically. It is noticed that the variable thickness of the surface has a leading consequence on the boundary layer progression along the surface. Moreover, the results of this study are not only useful for industrial applications but also present a basic understanding of the physical model.

Keywords: Micropolar fluid; variable thermal conductivity; thermal radiation; paraboloid of revolution.

1. Introduction

The boundary layer flow on a moving continuous surface is encountered in many engineering and manufacturing processes such as quenching of metallic sheets in a chilled bath, ion exchange liquid chromatography columns, subterranean chemical waste disposal, aerodynamic extrusion of plastic sheets etc. The problem of flow-induced due to a continuously moving surface with constant speed was originally explored by Sakiadis [1]. Crane [2] examined the influence of a stretched surface on the time-independent flow of a viscous fluid. The flow of a non-Newtonian fluid towards a stagnation point on a surface of stretching was explored by Ishak and co-workers [3]. Elbashbeshy and his associates [4] examined the effect of variable heat flux and heat generation on an unsteady porous stretching surface. Waqas et al. [5] reported the flow of a micropolar liquid induced by a nonlinear stretching sheet with convective heat condition. Nadeem and his associates [6-8] discussed the heat transfer in a micropolar fluid in different geometries.

In the engineering and industrial applications such as mechanical, civil, marine and aeronautical structures and designs the thickness of the sheet is not uniform and it plays an important role. The weight of structural elements can be reduced through the variable thickness and thus use of material is improved. Lee [9] is the pioneer to investigate the boundary layer flow along a slender body with non-uniform thickness by highlighting the flow through a needle with variable diameters. This model enables to describe the thickness and extensibility of the materials of the sheet which are used in many practical applications. Khader and Megahed [10] investigated the effects of varied thickness and partial slip on the boundary layer flow due to a sheet with nonlinear stretching. In their study, it is observed that the local skin friction coefficient improved with growing wall thickness parameter for the power-law index is less than one, while a reverse trend is noted when the power-law index exceeds unity. In a subsequent paper [11] they examined the thermal radiation and variable thermal conductivity effects on MHD flow caused by a stretching sheet. Daniel et al [12] explored the effect of thermal radiation coupled with Newtonian and Joule's heating on the boundary layer flow of a thermally stratified nanofluid past a nonlinearly stretching surface with a non-uniform thickness. They reported that the non-uniform thickness enhanced the fluid temperature and nanoparticle concentration. Several authors [see references 13-19] discussed the heat transfer effects on the boundary layer flows over a thin needle.

In aerospace science claims, the pointed edge of a rocket and aircraft are neither vertical nor inclined surfaces. These surfaces are of variable thickness and can be treated as the surface of revolution of a paraboloid. The study of fluid flow and heat transfer on these surfaces is more complex. In view of these, Davis and Werle [20] derived the numerical solutions to the problem governing the fluid flow along a paraboloid of revolution at zero angles of attack. Animasaun and Sandeep [21] studied the buoyancy induced flow of a nanofluid over an uhspr with non-uniform thermal conductivity and viscosity. They reported that the free convective flow along the surface with variable thickness is more reliable and suitable when the velocity power index is less than one. Makinde and Animasaun [22] examined the nonlinear thermal radiation on the chemically reactive alumina-water nanofluid containing gyrotactic-microorganism on an *uhspr*. In their model, the bio-convection is imposed assuming the diffusion coefficients of reactant A (bulk-fluid) and reactant B (catalyst at the surface) to be unequal. It is found that the local skin friction coefficient is maximum at greater values of thickness parameter while the local heat transfer rate is lesser at large values of temperature parameter. Gnaneswara Reddy and Sandeep [23] analyzed the transport phenomenon of energy and mass on MHD nanofluid flow past an uhspr. Koriko et al. [24] explored the partial slip impact on the boundary layer flow of Carreau nanofluid over an uhspr. They suggested that the buoyancy parameter is responsible for the rapid fall of temperature and increase of velocity distributions across the fluid layers. Recently, many researchers [25-31] studied numerically/analytically the influence of nanoparticles on heat transfer of a fluid through various flow models.

In spite of its several applications not much attention has been paid on the non-Newtonian fluid flows over a non-linear stretching surface with varied thickness. So, the main aim of this paper is to explore the effect of thermal radiation and buoyancy force on heat and mass transfer of a micropolar fluid flow over an *uhspr* immersed in a porous medium. A variable magnetic field is considered in this model. The content of this investigation is as follows. Mathematical formulation of the problem and boundary conditions are presented in section (2). Section (3) contains the method of solution. Section (4) deals with the results and discussion. The key features of this investigation are highlighted in Section (5).

2. Mathematical formulation

A steady boundary layer flow of an incompressible non-Newtonian micropolar fluid over an *uhspr* immersed in a Darcy porous medium is proposed. The Cartesian coordinate system is chosen such that *x*-axis is considered along the direction of the horizontal surface and *y*-axis perpendicular to it. It is assumed that the flow of the micropolar fluid under investigation prevails in the region $A\left(x+b\right)^{(1-m)/2} \le y \le \infty$, where *A* is a non-negative constant, *b* is a nonnegative parameter and *m* is the velocity power index pertaining to stretching as illustrated in the Fig.1. The flow is generated by stretching the surface of the paraboloid of revolution with a velocity $U_w = U_0 (x+b)^m$, where U_0 is reference velocity. It is pertinent to mention that the origin is not the starting point of the flow and the flow starts at the point $(A\left(b\right)^{(1-m)/2}, 0)$. The flow is exposed to a flexible magnetic field of strength $B = B_0 (x+b)^{(m-1)/2}$. It is also considered that the magnetic Reynolds number is very small and the electric field due to polarization of charges is negligible. The thermal conductivity of the fluid is taken to be variable. The effects of buoyancy, thermal radiation are incorporated in the study. The surface thermal convective conditions are considered in the investigation.

The governing expressions for micropolar fluid over an *uhspr* can be written as (see Refs. [22, 32]):

$$\frac{\partial u}{\partial x} + \frac{\partial v}{\partial y} = 0 \tag{1}$$

$$u\frac{\partial u}{\partial x} + v\frac{\partial u}{\partial y} = \frac{(\mu + k)}{\rho}\left(\frac{\partial^2 u}{\partial y^2}\right) + \frac{k}{\rho}\frac{\partial N}{\partial y} - \frac{\sigma B^2}{\rho}u - \frac{\nu}{k_1}u + g\beta_T (T - T_\infty) \tag{2}$$

$$u\frac{\partial N}{\partial x} + v\frac{\partial N}{\partial y} = \frac{\Omega}{\rho j}\frac{\partial^2 N}{\partial y^2} - \frac{k}{\rho j}\left(2N + \frac{\partial u}{\partial y}\right) \tag{3}$$

$$u\frac{\partial T}{\partial x} + v\frac{\partial T}{\partial y} = \frac{1}{\rho c_p}\frac{\partial}{\partial y}\left(k(T)\frac{\partial T}{\partial y}\right) + \frac{1}{\rho c_p}\frac{\partial q_r}{\partial y} \tag{4}$$

$$u\frac{\partial C}{\partial x} + v\frac{\partial C}{\partial y} = D_B\frac{\partial^2 C}{\partial y^2} \tag{5}$$

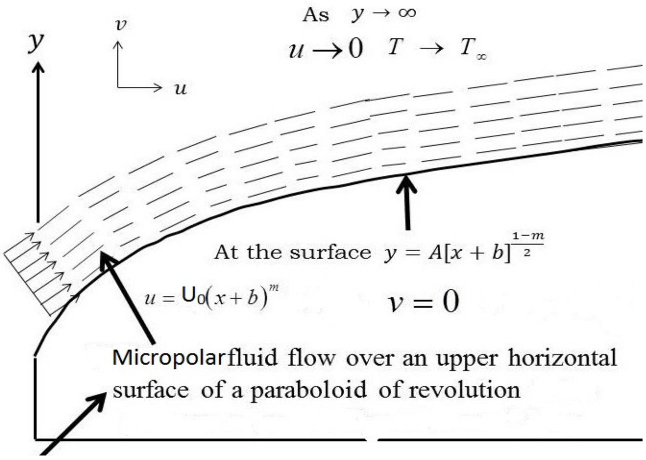

Fig. 1. Schematic flow geometry

The boundary conditions of the present flow are:

$$u = U_W = U_0(x+b)^m, V = 0, N = -n\frac{\partial u}{\partial y}, -k\frac{\partial T}{\partial y} = h_f(T_f - T), C = C_W \quad at \quad y = A(x+b)^{\frac{1-m}{2}} \tag{6}$$

$$u \to 0, N \to 0, T \to T_\infty, C \to C_\infty \quad as \quad y \to \infty \tag{7}$$

It is reported that the thermal conductivity K(T) approximately varies linearly with temperature in the range from $0^0 F$ to $400^0 F$ [see Kays [33]]. Following Arunachalam and Rajappa [34], K(T) is of the form

$$K(T) = k_\infty\left(1 + \delta\frac{T - T_\infty}{T_f - T_\infty}\right) \text{ where } \delta = \frac{k_w - k_\infty}{k_\infty} \tag{8}$$

Using the Rosseland approximation (Rosseland [35]), the radiative heat flux can be reduced in the form:

$$q_r = -\frac{4\sigma^*}{3k^*}\frac{\partial T^4}{\partial y} \tag{9}$$

Expanding T^4 in a Taylor series about T_∞ as:

$$T^4 = T_\infty^4 + 4T_\infty^3(T - T_\infty) + 6T_\infty^2(T - T_\infty)^2 + \ldots \tag{10}$$

and then neglecting higher order terms beyond the first degree in $(T - T_\infty)$, we get

$$T^4 = 4T_\infty^3 T - 3T_\infty^4 \tag{11}$$

In view of the equations (9) and (11), equation (4) reduces as follows:

$$u\frac{\partial T}{\partial x} + v\frac{\partial T}{\partial y} = \frac{1}{\rho c_p}\frac{\partial}{\partial y}\left(k(T)\frac{\partial T}{\partial y}\right) + \frac{16\sigma^* T_\infty^3}{3\rho c_p k^*}\frac{\partial^2 T}{\partial y^2} \tag{12}$$

3. Method of solution

To solve the equations (2) – (4), we consider the following similarity transformations:

$$\chi = \sqrt{\frac{U_0(m+1)(x+b)^{m-1}}{2\nu}}y \;,\; N = U_0(x+b)^{\frac{3m-1}{2}}\sqrt{\frac{U_0(m+1)}{2\nu}}H(\chi), u = U_0(x+b)^m F'(\chi)$$
$$v = -\sqrt{\frac{(m+1)\nu U_0(x+b)^{m-1}}{2}}\left[F(\chi) + \frac{m-1}{m+1}\chi F'(\chi)\right], \theta(\chi) = \frac{T - T_\infty}{T_f - T_\infty} \;,\; \phi(\chi) = \frac{C - C_\infty}{C_W - C_\infty} \tag{13}$$

In view of above similarity transformations, equations (2), (3), (5) and (12) are reduced to:

$$(1+\beta)F''' + FF'' - \frac{2m}{m+1}F'^2 + \beta H' - \frac{2}{m+1}(MF' + Da^{-1}F' - \lambda\theta) = 0 \tag{14}$$

$$\left(1+\frac{\beta}{2}\right)H'' - \beta(2H + F'') + FH' - \frac{3m-1}{m+1}F'H = 0 \tag{15}$$

$$(1+\delta\theta+\frac{4}{3}\mathrm{Nr})\theta''+\delta\theta'^2+\mathrm{Pr}F\theta'=0 \tag{16}$$

$$\phi''+ScF\phi'=0 \tag{17}$$

$$F(\alpha^*)=\alpha^*\frac{1-m}{1+m},\ F'(\alpha^*)=1, F'(\infty)=0 \tag{18}$$

$$H(\alpha^*)=-nF''(\alpha^*),\ H(\infty)=0 \tag{19}$$

$$\theta'(\alpha^*)=-Bi_1(1-\theta(\alpha^*)),\ \theta(\infty)=0 \tag{20}$$

$$\phi(\alpha^*)=1,\ \phi(\infty)=0 \tag{21}$$

The dimensionless governing equations (14) to (17) are depending on χ while the boundary conditions (18) to (21) are depending on α^*. In order to facilitate the computation transform the domain from $[\alpha^*,\infty)$ to $(0,\infty]$, so we introduce the function $F(\chi)=f(\chi-\alpha^*)=f(\eta)$, $H(\chi)=h(\chi-\alpha^*)=h(\eta)$, $\theta(\chi)=\theta(\chi-\alpha^*)=\theta(\eta)$ and $\phi(\chi)=\phi(\chi-\alpha^*)=\phi(\eta)$. Equations (14) – (17) together with the boundary conditions (18) – (21) reduce to

$$(1+\beta)f'''+ff''-\frac{2m}{m+1}f'^2+\beta h'-\frac{2}{m+1}(Mf'+Da^{-1}f'-\lambda\theta)=0 \tag{22}$$

$$(1+\frac{\beta}{2})h''-\beta(2h+f'')+fh'-\frac{3m-1}{m+1}f'h=0 \tag{23}$$

$$(1+\delta\theta+\frac{4}{3}\mathrm{Nr})\theta''+\delta\theta'^2+\mathrm{Pr}f\theta'=0 \tag{24}$$

$$\phi''+Scf\phi'=0 \tag{25}$$

The corresponding boundary conditions are

$$f(0)=\alpha^*\frac{1-m}{1+m},\ f'(0)=1,\ h(0)=-nf''(0),\ \theta'(0)=-Bi_1(1-\theta(0)),\ \phi(0)=1 \tag{26}$$

$$f'(\infty)=0,\ h(\infty)=0,\ \theta(\infty)=0,\ \phi(\infty)=0 \tag{27}$$

Physical quantities with engineering applications are the wall drag force C_f, the dimensionless wall couple stress M_w, measure of heat transfer Nu_x and measure of mass transfer Sh_x are defined by

$$C_f=\frac{\tau_w}{\rho u_w^2},\ M_W=\frac{M_x}{\rho u_w^2},\ Nu_x=\frac{(x+b)q_w}{k(T_W-T_\infty)},\ Sh_x=\frac{(x+b)m_w}{D(C_W-C_\infty)} \tag{28}$$

where

$$\tau_w=-((\mu+k)\frac{\partial u}{\partial y}+kN)_{y=A(x+b)^{\frac{1-m}{2}}},\quad m_x=\Omega(\frac{\partial N}{\partial y})_{y=A(x+b)^{\frac{1-m}{2}}}$$
$$q_w=-k(1+\frac{16\sigma^*T^3}{3Kk^*})(\frac{\partial T}{\partial y})_{y=A(x+b)^{\frac{1-m}{2}}},\quad m_w=-D(\frac{\partial c}{\partial y})_{y=A(x+b)^{\frac{1-m}{2}}} \tag{29}$$

Using equation (29) in equation (28), we obtain

$$C_f\sqrt{\mathrm{Re}_x}=-\sqrt{\frac{m+1}{2}}(1+\beta(1-n))f''(0) \tag{30}$$

$$M_w\,\mathrm{Re}_x=-\sqrt{\frac{m+1}{2}}(1+\frac{\beta}{2})h'(0) \tag{31}$$

$$\frac{Nu_x}{\sqrt{\mathrm{Re}_x}}=-\sqrt{\frac{m+1}{2}}(1+\frac{4}{3}Nr)\theta'(0) \tag{32}$$

$$\frac{Sh_x}{\sqrt{\mathrm{Re}_x}}=-\sqrt{\frac{m+1}{2}}\phi'(0) \tag{33}$$

The set of coupled nonlinear ODEs (22) - (25) together with boundary conditions (26) and (27) are solved using the powerful RKF-45 algorithm. The correctness of the numerical algorithm is ascertained by comparing our results, viz., $-f''(0)$ for various values of velocity power index m with those of Fang et al. [36] and Khader and Megahed [10] when $\beta=0$, $M=0$, $Da^{-1}=0$, $\lambda=0$, $\delta=0$, $Nr=0$, $\Pr=0$, $Sc=n=0$, $Bi_1\to\infty$ for $\alpha^*=0.5$ and $\alpha^*=0.25$ are tabulated in Table .1 and it reveals that our results are excellently agreed.

Table 1. Comparison between the results of the present and previous study for $-f''(0)$ when $\beta=M=Da^{-1}=\lambda=\delta=Nr=\Pr=Sc=n=0$, $Bi_1\to\infty$

m	$-f''(0)$					
	$\alpha^*=0.5$			$\alpha^*=0.25$		
	Fang et al. [36]	Khader and Megahed [10]	Present	Fang et al. [36]	Khader and Megahed [10]	Present
10.0	1.0603	1.0603	1.060306	1.1433	1.1433	1.143340
9.0	1.0589	1.0588	1.058938	1.1404	1.1404	1.140432
7.0	1.0550	1.0551	1.055127	1.1323	1.1322	1.132305
5.0	1.0486	1.0486	1.048614	1.1186	1.1186	1.118616
3.0	1.0359	1.0358	1.035949	1.0905	1.0904	1.090506
2.0	1.0234	1.0234	1.023484	---	---	---
1.0	1.0000	1.0000	1.000062	1.0000	1.0000	1.000062
0.5	0.9799	0.9798	0.979990	0.9338	0.9337	0.933881
0.0	0.9576	0.9577	0.957661	0.7843	0.7843	0.784320

4. Results and discussion

The objective of this part is to analyze the impact of free convection, variable thermal conductivity, and thermal radiation on the micropolar fluid flow over an *uhspr* immersed in a Darcy porous medium. The value of velocity power index (m) is taken to be less than one. The outcome of the analysis is discussed graphically through the flow variables for several sets of physical parameters.

It is clear from Fig. 2 (a) that as the inverse Darcy parameter Da^{-1} increases the fluid velocity is seen to diminish owing to the increased Darcy resistance offered by the porous medium. Higher values of Da^{-1} correspond to greater resistance to fluid flow resulting in deceleration of flow and thus the velocities are reduced and the associated hydrodynamic boundary layers are thinner. Fig. 2(b) displays the microrotation enhancement across the fluid region $0\le\eta\le1.768$ for an increment in Da^{-1} and subsequently it decreases with a reduction and later merge and ultimately satisfy the free stream condition. This is in conformity with the fact that porosity stabilizes the growth of the boundary layer. Besides smaller fluid mass, the obstruction due to the porous medium generates more heat and thus the temperature of the fluid enhances as Da^{-1} is incremented as illustrated in Fig. 2(c). In a similar fashion, the species concentration enhances with increasing Da^{-1} as shown in Fig. 2(d).

The effect of thermal buoyancy parameter λ on the flow field is plotted in Figs. 3(a)-(d). It is noted that increasing values of thermal buoyancy parameter have an enhancing effect on velocity and decreasing effect on temperature and species concentration profiles.

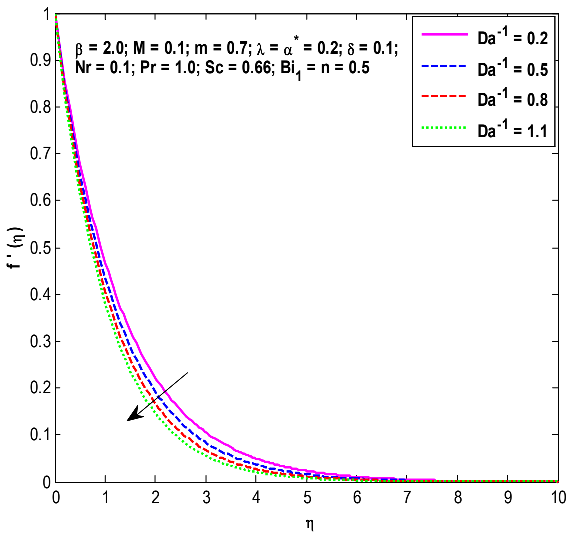

(a)

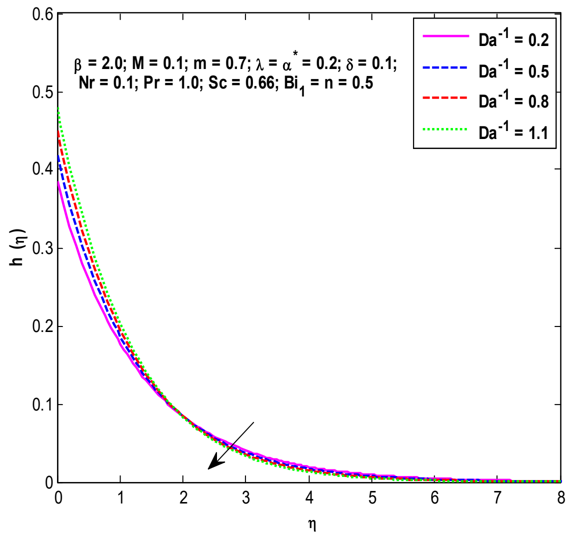

(b)

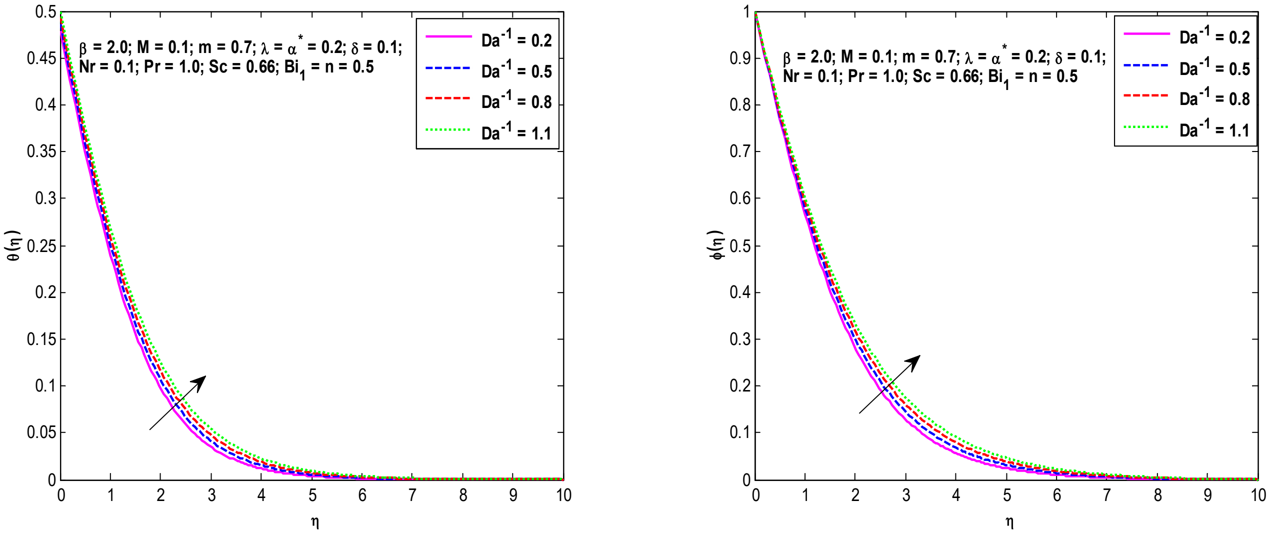

(c) (d)

Fig. 2. (a) Velocity (b) Microrotation (c) Temperature and (d) Concentration profiles for various values of Da^{-1}

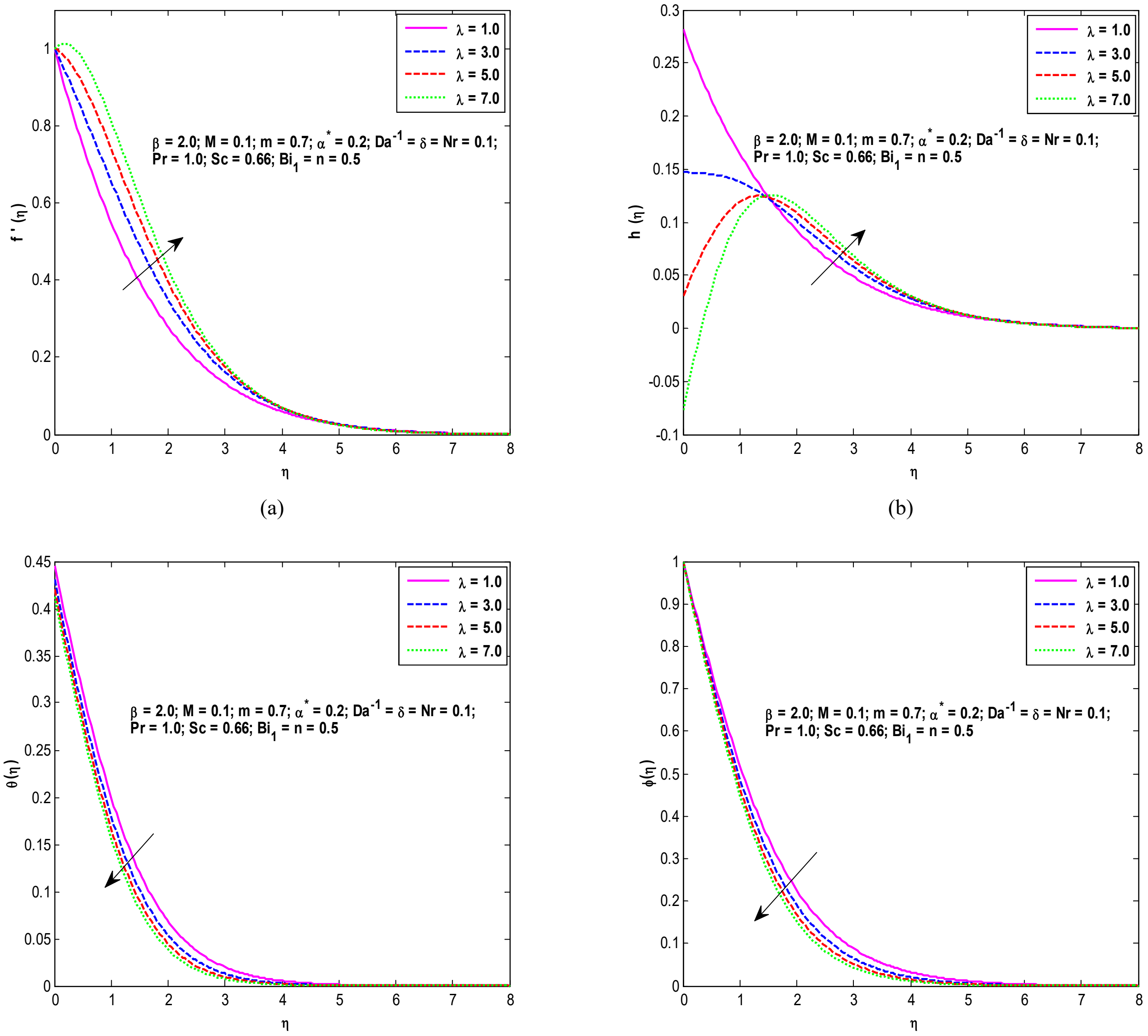

(a) (b)

(c) (d)

Fig. 3. (a) Velocity (b) Microrotation (c) Temperature and (d) Concentration profiles for various values of λ

Physically, buoyancy force acts as a favorable pressure gradient which accelerates the fluid within the boundary layer. Also, it is observed that the enhanced thermal buoyancy leads to the formation of thicker boundary layers. According to the analysis of Animasaun [37] and Shah et al. [38] the slope of a linear regression through data points (slp) on the wall is estimated as 0.119320743099865 and far upstream, that is at $\eta = 10$ it is 0.0000299410472835709 8 which accounts for the increase in the velocity. Microrotation is observed to diminish near the boundary $0 < \eta < 1.414$ and later it increases in $1.414 \le \eta < 6$ and eventually attains the free stream velocity as shown in Fig. 3(b). The slope of a linear regression through data points (slp) at the wall is -0.067246204058868 accounts for the decrease in micro-rotation while at $\eta = 2$ it is 0.0004029054399767807 accounts for the increase.

Figs. 4 (a) and (b) are the graphs of velocity and shear stress reflecting the influence of velocity power index m by taking $\lambda = 7$, $\alpha^* = 0.2$ and $M = 0.1$ and fixing the other parameters. It is interesting to note that a significant overshoot in velocity near the boundary is noticed for $m = 0.2$. With increment in m the overshoot of velocity is gradually reduced. The velocity distribution across fluid is seen to decrease with increase in m in the region $0 < \eta < 2.222$ and later shows a negligible enhancement reaching the far up stream condition as $\eta \to \infty$. The shear stress decreases sharply near the boundary and increases later which is corroborated with nature of velocity. We may conclude that velocity and shear stresses are greatly influenced by the wall thickness and buoyancy parameters as well as the power index.

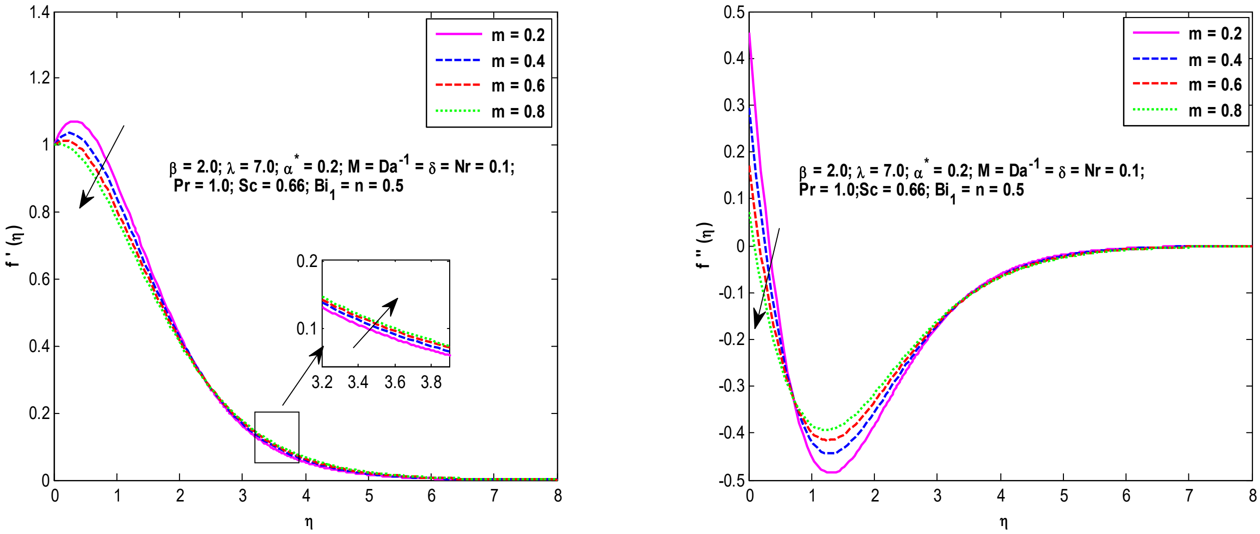

(a) (b)

Fig. 4. (a) Velocity and (b) Shear stress profiles for various values of m

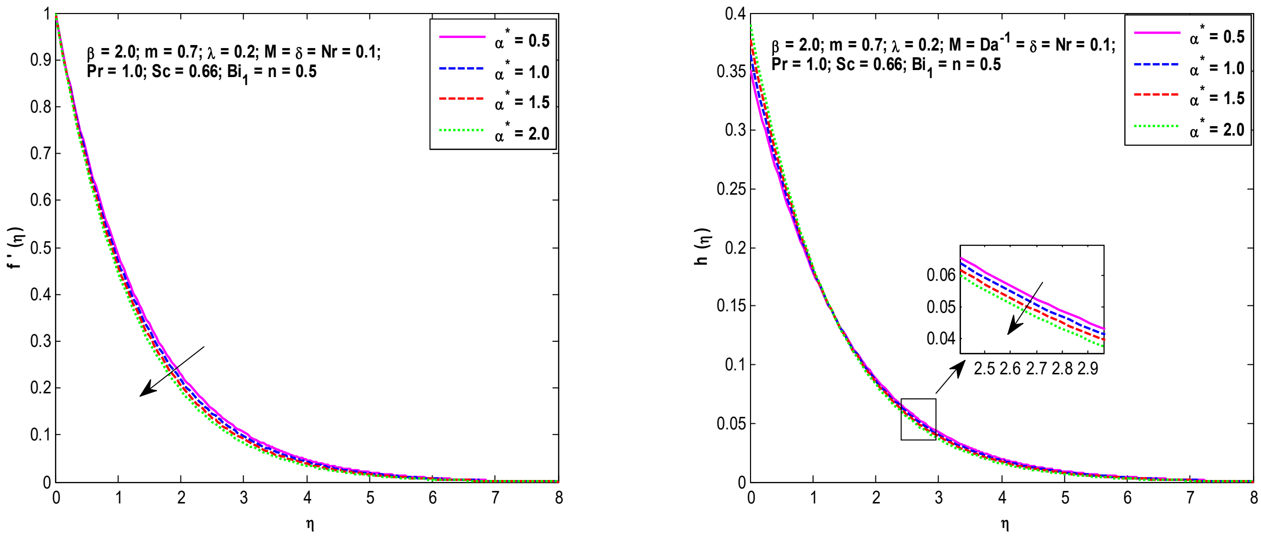

(a) (b)

Fig. 5. (a): Velocity and (b) Microrotation profiles for various values of α^*

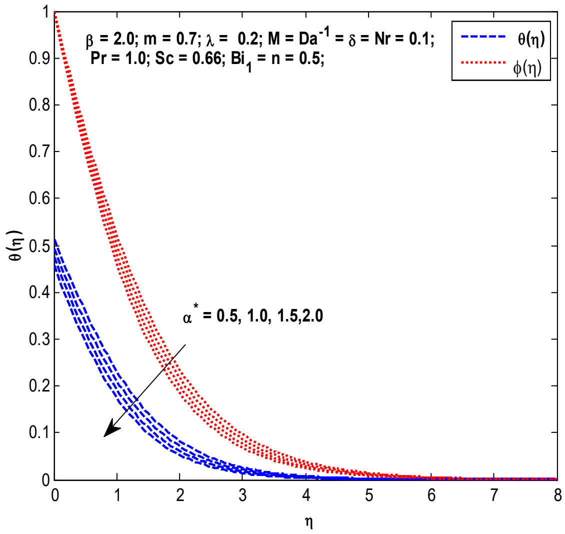

Fig. 5. (c) Temperature, concentration profiles for various values of α^*

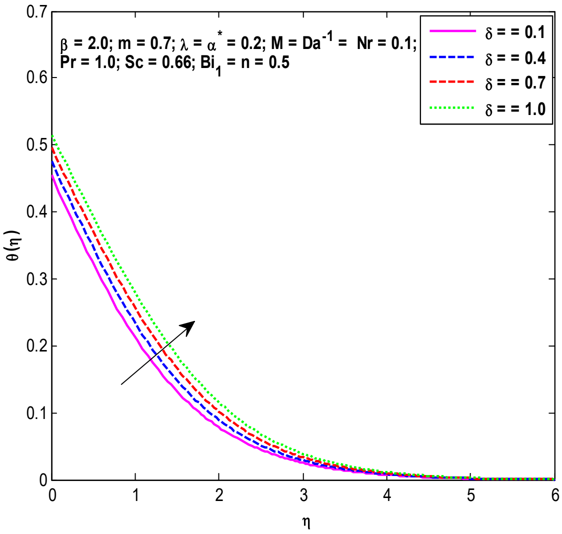

Fig. 6. Temperature profiles for various values of δ

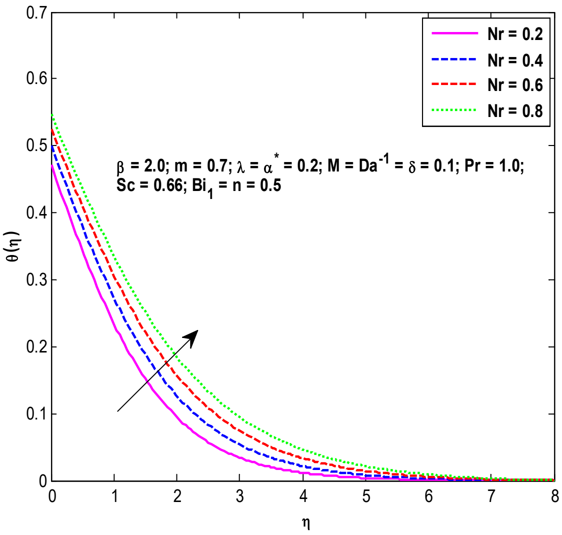

Fig. 7. Temperature profiles for various values of Nr

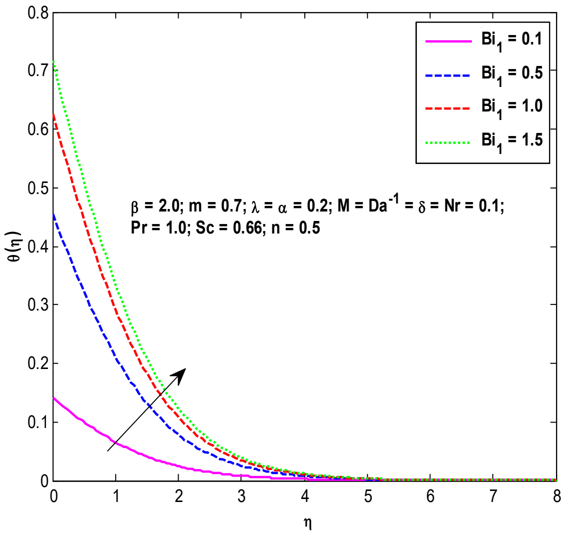

Fig. 8. Temperature profiles for various values of Bi_1

The effect of thickness parameter (α^*) on velocity, microrotation, temparature and concentration is plotted in Figs. 5(a)-(c) respectively. It is observed that all the profiles decrease monotonically from the surface to the ambient fluid for different values of the thickness parameter. Boundary layer becomes thinner when α^* is incremented. Also, the variation is prominent in the vicinity of the boundary.

The nature of variable thermal conductivity parameter δ on $\theta(\eta)$ is discussed in Fig. 6. It is observed that $\theta(\eta)$ rises with increment in δ as the fluid gets heated more due to the increased thermal conductivity of the fluid. Higher temperatures across the fluid layers occur for larger values of Nr as illustrated in Fig. 7. This is due to the release of thermal energy. The thickness of the corresponding thermal boundary layers enlarged.

Fig. 8 reports the variation of Bi_1 on $\theta(\eta)$ in the fluid region. Higher values of Bi_1 boost the $\theta(\eta)$ across the fluid region significantly. Physically, temperature rises due to the presence of the coefficient of heat transfer in the Biot number. Also, $Bi_1 = 0$, corresponds to the insulated wall where no heat transfer takes place at the wall and $Bi_1 \to \infty$, corresponds to the case of prescribed surface temperature.

Figs. 9 (a) – (d) represent the C_f, M_w, Nu_x and Sh_x versus magnetic field for a variation in the material parameter β. It is observed that C_f increases monotonically with the rise in the magnetic field strength and the values of C_f significantly decrease with increase in β. The profiles of skin friction are concave and radius of curvature of the curves increase with the increase in β. When $\beta = 4$ there is a 1.38 times reduction in skin friction to that of $\beta = 1$ for $M = 0.1$, while for $M = 1$ the reduction is 1.4 folds. Curves of couple stress are slightly convex showing a reduction with M and an enhancement with β. As β increases from 1 to 4 couple stress increases from -0.2867 to -0.1446 when $M = 0.1$ and from -0.4661 to -0.26 for $M = 1$. The Nusselt number and Sherwood number profiles are convex and their nature is qualitatively exactly opposite to that of the skin friction coefficient.

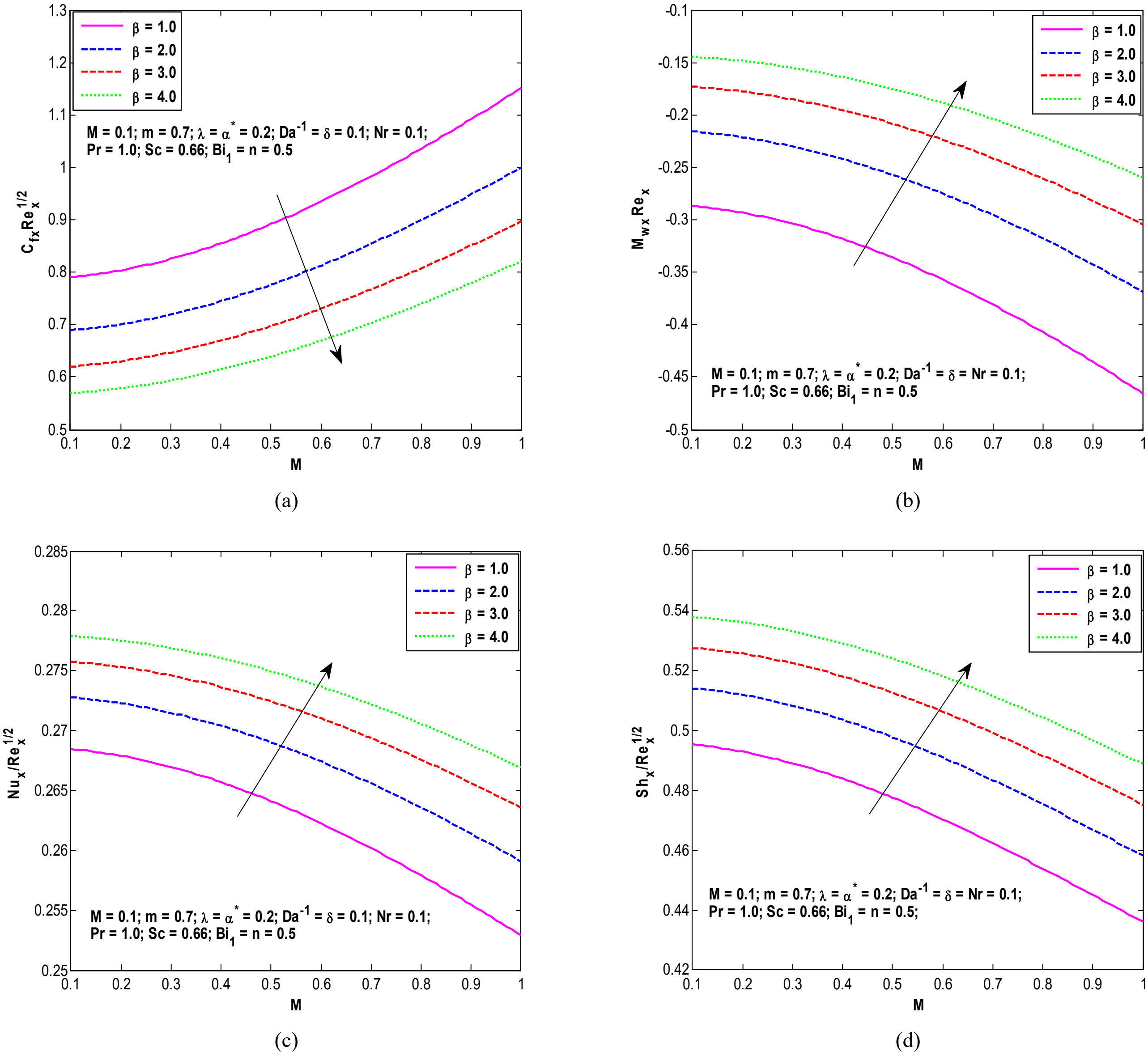

Fig. 9. (a) Skin friction (b) Couple stress coefficient and (c) Nusselt number and (d) Sherwood number distribution with β and M

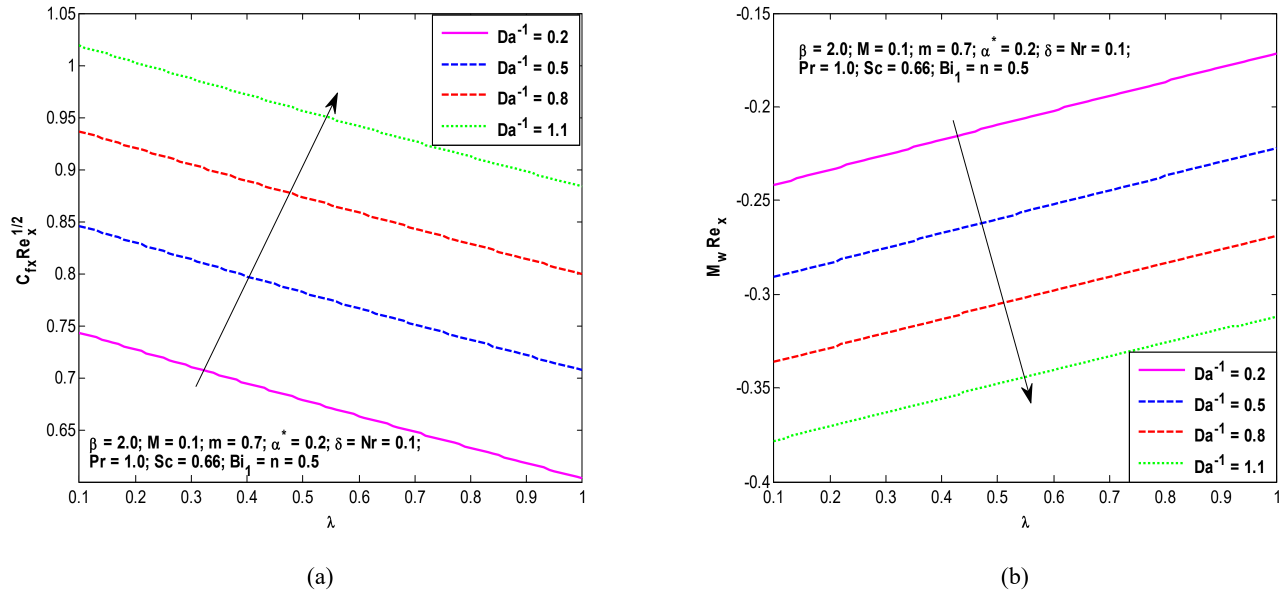

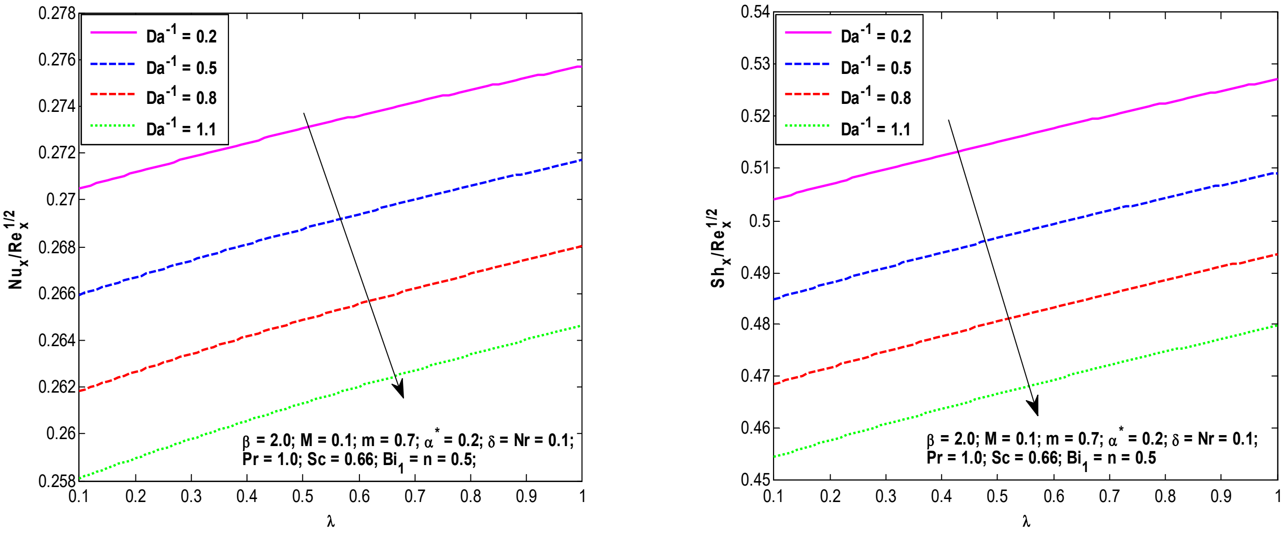

(c) (d)

Fig. 10. (a) Skin friction (b) Couple stress coefficient and (c) Nusselt number and (d) Sherwood number distribution with Da^{-1} and λ

Figs. 10(a)-(d) represent the C_f, M_w, Nu_x and Sh_x versus thermal buoyancy parameter (λ) for a variation in the inverse Darcy parameter (Da^{-1}) Surface drag coefficient is seen to decrease linearly as (Da^{-1}) increases while the ratio of thermal buoyancy decreases. It is observed that the couple stress coefficient increases linearly with (λ) and the values of couple stress coefficient significantly diminish with an increase in (Da^{-1}). For the same set of variables, Nusselt number and Sherwood number qualitatively show the same behavior as that of the couple stress coefficient.

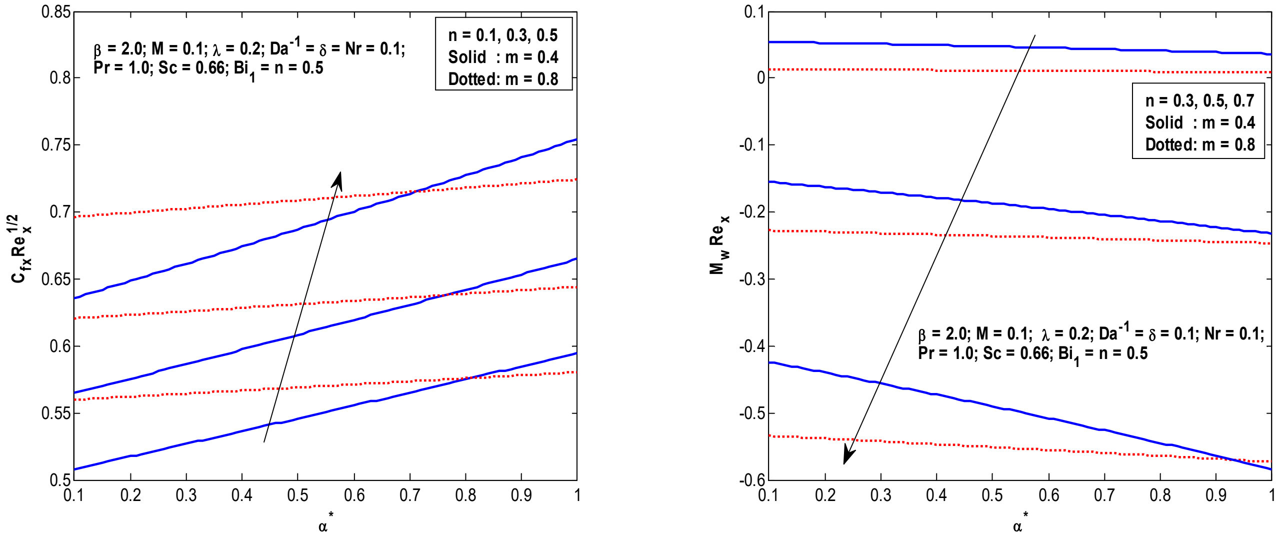

(a) (b)

Fig. 11. (a) Skin friction and (b) Couple stress coefficients with n, m and α^*

Figs. 11 (a) and (b) respectively show the relationship between the C_f, M_w, and thickness parameter α^* for different variation in n when $m = 0.4$ and $m = 0.8$. The surface drag enhances linearly for an increment α^*, n and m. The couple stress parameter qualitatively shows an opposite behavior for the same sets of variations in n, m, and α^*.

5. Conclusions

This investigation brings out a mathematical model to elucidate the effect of variable thermal conductivity, radiative heat on the flow of a micropolar fluid on the *uhspr* through a porous medium. The exactness of the present results is corroborated by comparing with the already published investigations. The analysis shall be helpful to understand the characteristics of heat and mass transfer in the flow over an aircraft or on the car bonnet. Some of the findings of the study are:

- Thickness parameter, velocity power index and buoyancy ratio have a significant influence on the velocity distribution and shear force in the fluid region.
- Material parameters have an increasing influence on the velocity while the magnetic and inverse Darcy and wall thickness parameters show a reverse effect.
- Overshoot of velocity is noticed for higher values of thermal buoyancy ratio parameter.
- Parameters of thermal radiation, variable thermal conductivity and Biot number have an increasing influence on the temperature distribution.
- Surface drag coefficient is decreased with material parameter while the magnetic parameter shows an increasing tendency. Couple stress, Nusselt and Sherwood numbers depict an exact trend to that of surface drag.

Nomenclature

A, b	Non negative constants
u, v	Velocity components along x, y-axis
$Bi_1 = h_f / \left(K\sqrt{\dfrac{zU_0(x+b)^{m-1}}{(m+1)v}}\right)$	Heat transfer Biot number
C	Fluid concentration
C_w	Surface concentration
c_f	Wall drag force
c_p	Specific heat at constant pressure
C_∞	Ambient fluid concentration
$Da^{-1} = \dfrac{v}{k_1 U_0 (x+b)^{m+1}}$	Inverse Darcy number
f	Dimensionless stream function
f'	Dimensionless velocity
$Gr_x = \dfrac{g\beta_T (T_f - T_\infty)(x+b)^s}{v^2}$	
g	Acceleration due to gravity
h_f	Convective heat transfer coefficient
$j = 2v / (m+1)ax^{m-1}$	Micro-inertia density
k^*	Mean absorption coefficient
k_1	Permeability of the porous medium
k	Vortex viscosity
k_w	Wall thermal conductivity
k_∞	Ambient thermal conductivity
$Sc = \upsilon / D$	Schmidt number
$M = \dfrac{\sigma B_0^2}{\rho U_0}$	Magnetic field parameter
M_w	Dimensionless wall couple stress
m_x	Wall couple stress
m_w	Mass flux
N	Microrotation
Nu_x	Measure of heat transfer
$Nr = \dfrac{4\sigma^* T_\infty^2}{k_\infty k^*}$	Thermal radiation parameter
$\Pr = \dfrac{\rho c_p v}{k_\infty}$	Prandtl number
q_w	Surface heat flux
q_r	Radiative heat flux
$\mathrm{Re}_x = \dfrac{U_w(x+b)}{v}$	Reynolds number
Sh_x	Measure of mass transfer
T_∞	Ambient fluid temperature
T	Fluid Temperature
T_f	Convective fluid temperature

Greek symbols

$\lambda = \dfrac{Gr_x}{\mathrm{Re}_x^2}$	Thermal buoyancy ratio parameter
$\alpha^* = A\sqrt{\dfrac{(m+1)U_0}{2v}}$	Wall thickness parameter
ϕ	Dimensionless concentration
δ	Thermal conductivity parameter
β_T	Coefficient of thermal expansion
θ	Dimensionless temperature
τ_w	Wall shear stress
v	Kinematic viscosity
ρ	Fluid density
μ	Dynamic viscosity
$\Omega = \left(\mu + \dfrac{k}{2}\right)j = \mu\left(1 + \dfrac{\beta}{2}\right)j$	Spin-gradient viscosity
$\beta = \dfrac{k}{\mu}$	Material parameter
σ^*	Stefan-Boltzmann constant
σ	Electrical conductivity

Subscripts

∞	Condition at free stream

Conflict of Interest

The author(s) declared no potential conflicts of interest with respect to the research, authorship and publication of this article.

Funding

The author(s) received no financial support for the research, authorship and publication of this article.

References

[1] B.C. Sakiadis, Boundary-layer behavior on continuous solid surfaces: I. Boundary-layer equations for two dimensional and axis symmetric flow, *AIChE Journal*, 26 (1961) 221-227.
[2] L.J. Crane, Flow past a stretching plate, *Journal of Applied Mathematics and Physics*, 21 (1970) 645-647.
[3] Ishak, R. Nazar and I. Pop, Mixed convection stagnation point flow of a micropolar fluid towards a stretching sheet, *Meccanica*, 43 (2008) 411-418.
[4] E.M.A. Elbashbeshy, D.M. Yassmin and A.A. Dalia, Heat transfer over an unsteady porous stretching surface embedded in a porous medium with variable heat flux in the presence of heat source or sink, *African Journal of Mathematics and Computer Science Research*, 3(5) (2010) 68-73.
[5] M. Waqas, M. Farooq, M.I. Khan, A. Alsaedi, T. Hayat and T. Yasmeen, Magnetohydrodynamic (MHD) mixed convection flow of micropolar liquid due to nonlinear stretched sheet with convective condition, *International Journal of Heat and Mass Transfer*, 102 (2016) 766-772.
[6] N. Abbas, S. Saleem, S. Nadeem, A.A. Alderremy, and A.U. Khan, on stagnation point flow of a micro polar nanofluid past a circular cylinder with velocity and thermal slip, *Results in Physics*, 9 (2018) 1224-1232.
[7] S. Nadeem, Z. Ahmed, S. Saleem, The effect of variable viscosities on micro-polar flow of two nanofluids, *Zeitschrift für Naturforschung A*, 71(12) (2018) 1121–1129.
[8] S. Nadeem and S. Saleem, Analytical study of third grade fluid over a rotating vertical cone in the presence of nanoparticles, micropolar liquid due to nonlinear stretched sheet with convective condition, *International Journal of Heat and Mass Transfer*, 85 (2015) 1041-1048.
[9] L.L. Lee, Boundary layer over a thin needle, *Physics of Fluids*, 10 (1967) 822-828.
[10] M.M. Khader and A.M. Megahed, Numerical solution for boundary layer flow due to a nonlinearly stretching sheet with variable thickness and slip velocity, *The European Physical Journal Plus*, 128 100 (2013).
[11] M.M. Khader, M.M. Babatin, A. Eid and M. Megahed, Numerical study for simulation the MHD flow and heat-transfer due to a stretching sheet on variable thickness and thermal conductivity with thermal radiation, *Applied Mathematics*, 6 (2015) 2045-2056.
[12] Y.S. Daniel, Z.A. Aziz, Z. Ismail, F. Salah, Thermal stratification effects on MHD radiative flow of nanofluid over nonlinear stretching sheet with variable thickness, *Journal of Computational Design and Engineering*, 2 (2018) 232–242.
[13] T. Cebeci, and T.Y. Na, Laminar free-convection heat transfer from a needle, *Physics of Fluids*, 12 (1969) 463-465.
[14] Md Tausif .Sk, K. Das and P. K. Kundu, Consequences of nanoparticle diameter and solid–liquid interfacial layer on the SWCNT/EO nanofluid flow over various shaped thin slendering needles, *Chinese Journal of Physics*, in press, Doi: 10.1016/j.cjph.2018.06.016.
[15] R. Ahmad, M. Mustafa, S. Hina, Buongiorno's model for fluid flow around a moving thin needle in a flowing nanofluid: A numerical study, *Chinese Journal of Physics*, 55 (2017), 1264-1274.
[16] J.L.S. Chen, Mixed convection flow about slender bodies of revolution, *J. Heat Transf.*, 109 (1987) 1033-1036.
[17] S.L. Lee, T.S. Chen and B.F. Armaly, Mixed convection along vertical cylinders and needles with uniform surface heat flux, *Journal of Heat Transfer*, 109 (1987) 711-716.
[18] C.Y. Wang, Mixed convection on a vertical needle with heated tip, *Physics of Fluids*, 2 (1990) 622-625.
[19] S. Ahmad, N.M. Arifin, R. Nazar and I. Pop, Mixed convection boundary layer flow along vertical thin needles: assisting and opposing flows, *International Communications in Heat and Mass Transfer*, 35 (2008) 157-162.
[20] R.T. Davis and M.J. Werle, Numerical solutions for laminar incompressible flow past a paraboloid of revolution, *American Institute of Aeronautics and Astronautics*, 10 (2015) 1224–1230.
[21] I.L. Animasaun and N. Sandeep, Buoyancy induced model for the flow of 36 nm alumina-water nanofluid along upper horizontal surface of a paraboloid of revolution with variable thermal conductivity and viscosity, *Power Technology*, 301 (2016) 858-867.
[22] O.D. Makinde and I.L. Animasaun, Bioconvection in MHD nanofluid flow with nonlinear thermal radiation and quartic autocatalysis chemical reaction past an upper surface of a paraboloid of revolution, *International Journal of Thermal Sciences*, 109 (2016) 159-171.
[23] M. Gnaneswara Reddy and N. Sandeep, Computational modelling and analysis of heat and mass transfer in MHD flow past the upper part of a paraboloid of revolution, *The European Physical Journal Plus*, 132 222, (2017).
[24] O.K. Koriko, I.L. Animasaun, B. Mahantesh, S. Saleem, G. Sarojamma and R. Sivaraj, Heat transfer in the flow of blood-gold Carreau nanofluid induced by partial slip and buoyancy, *Heat Transfer-Asian Research* ,47(6) (2018) 806-823.
[25] Z. Li, M. Sheikholeslami, A. Shafee, S. Saleem, A.J. Chamkha, Effect of dispersing nanoparticles on solidification process in existence of Lorenz forces in a permeable media, *Journal of Molecular Liquids*, 266 (2018) 181-193.

[26] S. Mamatha Upadhya, C.S.K.Raju, S. Saleem, A.A. Alderremy, Mahesha, Modified Fourier heat flux on MHD flow over stretched cylinder filled with Dust, Graphene and silver nanoparticles, *Results in Physics*, 9 (2018) 1377-1385.
[27] P.V. Venkateswarlu and S. Narayana, Chemical reaction and radiation absorption effects on the flow and heat transfer of a nanofluid in a rotating system, *Applied Nanoscience*, 5 (2015) 351-360.
[28] M. Sheikholeslami, A. Ghasemi, Z. Li, A. Shafee, S. Saleem, Influence of CuO nanoparticles on heat transfer behavior of PCM in solidification process considering radiative source term, *International Journal of Heat and Mass Transfer*, 126(A) (2018) 1252-1264.
[29] P.V. Satya Narayana, S.M. Akshit, J.P. Ghori and B. Venkateswarlu, Thermal radiation effects on an unsteady MHD nanofluid flow over a stretching sheet with non-uniform heat source/sink, *Journal of Nanofluids*, 8 (2017) 1-5.
[30] Z. Li, M. Sheikholeslami, A.J. Chamkha, Z.A. Raizah, S. Saleem, Control Volume Finite Element Method for nanofluid MHD natural convective flow inside a sinusoidal annulus under the impact of thermal radiation, *Computer Methods in Applied Mechanics and Engineering*, 338 (2018) 618-633.
[31] K. Sreelakshmi G. Sarojamma, Heat transfer analysis in the non-orthogonal flow of a non-Newtonian nanofluid with non-linear thermal radiation, *Transactions of A. Razmadze Mathematical Institute*, 172 (2018) 606–618.
[32] O.K. Koriko and I.L. Animasaun, New similarity solution of micropolar fluid flow problem over an *uhspr* in the presence of quartic kind of autocatalytic chemical reaction, *Frontiers in Heat and Mass Transfer*, 26 (2017) 1-13.
[33] W.M. Kays, *Convective heat and mass transfer*, New York: McGraw-Hill, (1966).
[34] M. Arunachalam and N.R. Rajappa, Thermal boundary layer in liquid metals with variable thermal conductivity, *Applied Scientific Research*, 34 (1978) 179-187.
[35] S. Rosseland, *Astrophysik und Atom-Theoretische Grundlagen*, Springer Verlag, Berlin, (1931) 41-44.
[36] T. Fang, J.I. Zhang and Y. Zhong, Boundary layer flow over a stretching sheet with variable thickness, *Applied Mathematics and Computation*, 218 (2012) 7241-7252.
[37] I.L. Animasaun, Double diffusive unsteady convective micropolar flow past a vertical porous plate moving through binary mixture using modified Boussineq approximation, *Ain Shams Engineering Journal*, 7 (2016) 755-765.
[38] N.A. Shah, I.L. Animasaun, R.O. Ibraheem, H.A. Babatunde, N. Sandeep and I. Pop, Scrutinization of the effects of Grashof number on the flow of different fluids driven by convection over various surfaces, *Journal of. Molecular Liquids*, 249 (2018) 980-990.